Tealdi, C., Lavrentiev, M. Y., Mohn, C. E., & Allan, N. L. (2016). Perovskite solid solutions–a Monte Carlo study of the deep earth analogue (K, Na)MgF_3. *Journal of Structural Chemistry*, *57*(2), 257-266. https://doi.org/10.1134/S0022476616020037

Perovskite solid solutions – a Monte Carlo study of the deep Earth analogue (K, Na)MgF_3

C. Tealdi[a], M.Y. Lavrentiev[b], C.E. Mohn[c] and N.L. Allan[d]

[a] Department of Chemistry, University of Pavia, and INSTM, Viale Taramelli 16, I-27100, Pavia, Italy

[b] United Kingdom Atomic Energy Authority, Culham Science Centre, Abingdon, Oxon OX14 3DB, United Kingdom

[c] Centre for Earth Evolution and Dynamics (CEED), University of Oslo, PO Box 1033 Blindern, N-0315, Oslo, Norway

[d] School of Chemistry, University of Bristol, Bristol, BS8 1TS, United Kingdom

Abstract

Understanding the behaviour of solid solutions over wide ranges of temperature and pressure remains a major challenge to both theory and experiment. Here we report a detailed exchange Monte Carlo study using a classical ionic model of the model perovskite parascandolaite-neighborite (K,Na)MgF_3 solid solution and its end-members for temperatures in the range 300-1000 K and pressures from 0-8 GPa. Full account is taken of the local environment of the individual cations, clustering and thermal effects. Properties considered include the crystal structure, phase transitions, the thermodynamics of mixing and the non-ideality of the solid solution. Clustering of the potassium ions is examined via a short-range order parameter. Where experimental data are available for comparison, agreement is very good.

1. Introduction

Solid solutions and phase stability continue to present considerable challenges for theory. Energy differences between different phases can be small and subtle cation ordering effects can be often crucial in determining phase stability and thermodynamic and chemical properties. In this paper we turn our attention to the perovskite solid solution (K,Na)MgF_3. This solution is not only an excellent test of any theoretical model, but also serves as a useful analogue for the silicate perovskite (Mg, Fe)(Al,Si)O_3, which is a dominant phase under the conditions of the lower mantle of the Earth (pressure > 25 GPa, temperature > 2000 K) [1-4]. Because of the difficulties of generation of lower mantle conditions experimentally, possible structural phase transitions and substitution mechanisms in silicate perovskites still remain the subject of extensive debates, experimental and theoretical studies [5-10]. Neighborite $NaMgF_3$ [11] is isoelectronic and isostructural with $MgSiO_3$; the ratios of the formal cation charges are the same in both compounds (1:2) and the ratio of their ionic radii are about the same. $KMgF_3$ was until very recently known only as a synthetic crystal but has now been identified as the new mineral parascandolaite, found as a volcanic sublimate at Vesuvius [12].

$KMgF_3$ is a cubic perovskite (Figure 1a), while in $NaMgF_3$ there is an orthorhombic distortion such that the Mg-F-Mg bridges linking the MgF_6 octahedra are not linear (Figure 1b). The simplest rationalization of this distortion is in terms of the ionic radii of K^+, Na^+ and F^- and the radius ratio rules (the so-called 'tolerance factor') is possible [13, 14]. The Na^+ cation is too small to touch the twelve neighbouring anions in a cubic structure and the Mg-F-Mg links bend, tilting the MgF_6 octahedra to bring further anions into contact with the A cations. An extensive NMR and X-ray diffraction study of the effect of the A-site cation radius on the ordering of BX_6 octahedra in (K,Na)MgF_3 has recently been reported by Martin *et al.* [14]. The exact nature and order of structural transitions along the $Na_{1-x}K_xMgF_3$ series continue to be the subject of a large number of experimental and theoretical studies [15-26]. Smith *et al.* [18] have complemented an experimental study of (K,Na)MgF_3 with a molecular dynamics simulation based on pair potentials. Their results for the phase transitions in $Na_{1-x}K_xMgF_3$ for $0 \leq x \leq 0.4$ are in broad agreement with earlier results of Zhao *et al.* [15-17]. For neighborite $NaMgF_3$ a single structural phase transition from orthorhombic to the cubic phase at about 1038 K

was found, while for the solid solution $Na_{1-x}K_xMgF_3$, the system undergoes two transitions with increasing temperature, going from orthorhombic to tetragonal and then from tetragonal to cubic phase. However, their study used a small simulation box of 320 atoms and the solid solution $Na_{1-x}K_xMgF_3$ was obtained by replacing Na ions with K ions at sites selected at random. This approach assumes ideality, and misses possible clustering and other short-range order effects.

The end members $KMgF_3$ and $NaMgF_3$ have recently been investigated using first principles methods. Umemoto *et al.* [27] used density functional theory to investigate pressure-induced structural transitions in $NaMgF_3$, using the quasiharmonic approximation to extend their treatment to nonzero temperatures. $NaMgF_3$ transforms at pressures over approximately 20 GPa to the same post-perovskite structure also adopted by $MgSiO_3$ at high pressure. For $KMgF_3$ Vaitheeswaran *et al.* [26] performed a combined experimental and ab initio density functional study and concluded the cubic phase is stable even at 40 GPa. However, such studies are difficult to expand to intermediate members of the $(K,Na)MgF_3$ solid solution because of limitations of small simulation cell sizes in such first principles methods. In addition temperature effects in solid solutions are currently very difficult to study *ab initio*. For this, computationally fast methods that allow study of many configurations in a large supercell are essential.

A key feature of our computational methodologies for solid solutions [28-32] is the sampling of many different arrangements of atoms, allowing for the exchange of atoms located at crystallographically inequivalent positions. The *local* environment of each ion and the local structural movements (relaxation), which accompany any exchange of atoms and reduce considerably the energy associated with any such interchange, are taken into account. Local effects due to clustering are not averaged out. An advantage, compared with fitted Hamiltonians, is that elevated temperatures (vibrational terms) and high pressures are readily taken into account; no refitting is required.

2. Theoretical Methods

Monte Carlo simulations

As a starting point we describe the classical Monte Carlo technique for atomistic simulations and then discuss how this has been extended here. During one step of the Monte Carlo simulation a random decision is made to alter one of the variables of the

calculation, which may either be an atomic position or the cell dimensions, i.e. all simulations are carried out within the *NPT* ensemble and lattice vibrations are automatically included [33]. The magnitude of the change is also chosen at random, but within a specified amount and governed by the variables r_{max} and v_{max} respectively. The magnitude of these variables is adjusted automatically so that the magnitude of the acceptance/rejection ratio is 0.3. After each move/volume alteration the change in energy is calculated and a decision whether to accept or reject this is made according to the standard Metropolis scheme [34]. We have extended this approach to allow for the atomic configuration to evolve during the simulation [28]. In addition to random movements of atoms, or cell volume change a further possibility is to exchange two cations (here Na^+ and K^+) chosen at random again with the acceptance/rejection decision made using the Metropolis scheme.

Unfortunately in practice such a simple scheme is impractically slow for the (Na,K)MgF_3 solid solution, since the efficiency of the cation exchange is very low due to the difference in size between sodium and potassium. For example, at 500 K the rate of successful exchanges of Na and K is only 3.7 %; this rate falls even further down to 0.4 % at 300 K. Low exchange rate slows down the equilibration, so that special methods are necessary to increase the rate of successful exchanges. To speed up sampling of the configurations we have applied the biased sampling technique, widely used in the simulation of molecules and polymers (see, e.g., ref. 33). Our exchange-biased Monte Carlo has been successfully applied to systems such as the CaO/MgO solid solution [30], spinels [35], and garnet solid solutions [36]. Instead of considering a single trial exchange, a set of trial exchanges is picked at random. Suppose an exchange take place between atoms A and B. First, k pairs $\{A^i, B^i, i=1,\ldots, k\}$ are randomly chosen. We denote the system energy in the initial configuration as U_{old} and the energy of the system after exchange of atoms in the ith pair as U^i_{new}. One of the new configurations is then chosen with probability

$$p_i = \frac{\exp(-\beta(U^i_{new} - U_{old}))}{W_{new}}, \beta = (kT)^{-1}, \quad (1)$$

where

$$W_{new} = \sum_{l=1}^{k} \exp(-\beta(U^l_{new} - U_{old})) \quad (2)$$

The chosen configuration i (that after the exchange of the ith pair) with energy $U^i_{new} \equiv U_{new}$ is

then the trial configuration. However, the usual Monte Carlo metropolis acceptance rule cannot be directly applied. Instead, starting from the new configuration, a further k-1 pairs A^j, B^j, j=1,…, k-1 are chosen. Denoting the energy of the system after exchange of atoms in the jth pair U_{old}^j, we evaluate the expression

$$W_{old} = \exp(-\beta(U_{old} - U_{new})) + \sum_{j=1}^{k-1} \exp(-\beta(U_{old}^j - U_{new})) \quad (3)$$

Fulfilling detailed balance, the criterion for the acceptance of the new configuration is

$$acc(old \rightarrow new) = \min\left[1, \exp(-\beta(U_{old} - U_{new}))\frac{W_{new}}{W_{old}}\right] \quad (4)$$

Use of the exchange-bias technique with k = 100 makes possible Monte Carlo simulations with a successful exchange rate of Na^+ and K^+ in (Na,K)MgF_3 of ≈ 50 % at 500 K and higher and as large as 11% at 300 K. All calculations were performed using a periodic orthorhombic simulation cell, shown in Figure 2, containing 256 formula units (1280 ions), and consisted of 10×10^7 steps in the data accumulation stage following an initial equilibration stage of 4×10^7 steps.

Potentials

All calculations are based on the ionic model using two-body potentials to represent the short-range forces (for a full discussion of this well-known model see, for example, ref. 37). Ions are assigned their conventional charges, i.e., +1 for Na and K, +2 to Mg and −1 for F. We use the set of electron gas potentials for ternary fluorides AMF_3 (A=Li-Cs, B=Ca-Ba) developed and tested by Allan *et al.* [13] with one modification in that the shell model was not used, i.e., we work within a rigid ion model. These potentials have also been employed in studies of NaF and KF at high pressure [38, 39], and have also been validated by subsequent density functional calculations for a number of fluoride perovskites [40]. Here, for ease of use, the electron gas potentials have been fitted to Buckingham forms and these are collected together in Table 1.

3. Results and Discussion

End Members Parascandolaite and Neighborite

We start with the structures of the end members themselves and a comparison with

experiment [14, 15, 19, 41]. Static energy minimizations for parascandolaite $KMgF_3$ and neighborite $NaMgF_3$ were first performed, and the results are presented in Table 2. The predicted structures are those observed (cubic for $KMgF_3$, orthorhombic for $NaMgF_3$) and there is excellent agreement with the experimental unit cell parameters. Unit cell parameters as a function of temperature for $KMgF_3$ and $NaMgF_3$, generated from the Monte Carlo simulations, are shown in Figure 3. The temperature range of our simulations is restricted from above by the experimental melting points, 1303 K for $NaMgF_3$ [42] and 1343 K for $KMgF_3$ [43].

For $KMgF_3$, no structural phase transitions were observed in the simulations, in agreement with experiment. The crystal structure is cubic, with differences between the pseudo-cubic unit cell parameters not exceeding 0.002 Å at all temperatures (Figure 3). For $NaMgF_3$, there is a transition from the orthorhombic to the cubic structure at about 1100 K, very close to the experimentally observed temperature of 1038 K [15, 18]. Chao *et al.* [11] and Wood *et al.* [20] have suggested that an intermediate tetragonal phase exists in a narrow temperature range below that of the formation of the cubic phase. We cannot confirm this observation at zero pressure as the difference between the longest and shortest unit cell parameters at 1100 K and 1200 K does not exceed 0.003 Å in our simulations (see Figure 3). It is worth noting that experimentally Zhao [17] concluded there is no tetragonal phase at atmospheric pressure.

With increasing pressure, the transition from orthorhombic to cubic occurs at progressively higher temperatures. The simulations possibly suggest that the nature of the structural phase transitions in the end member $NaMgF_3$ changes. Figure 4 shows that at 4 GPa and 8 GPa and two of the three lattice parameters are very close and larger than the third at the highest temperatures. This indicates at least the possible formation of a tetragonal phase approximately 200 K below the transition to the cubic form, which is in disagreement with the X-ray studies of Zhao *et al.* [17, 44], who found a positive slope of about 45 K/GPa for the orthorhombic-cubic phase boundary and no intermediate tetragonal phase in $NaMgF_3$ at pressures up to 9 GPa. Our calculated value for the phase boundary of the orthorhombic-tetragonal transition is approximately 50 K/GPa. Chen *et al.* [22] have performed a more recent experimental study and commented that "pressure seems to enhance the possibility of … a tetragonal intermediate phase between the orthorhombic and cubic phases." The pseudocubic cell

volume of $NaMgF_3$ does not demonstrate singularities with increasing temperature, in agreement with experiment [15] (Figure 5) and suggesting a higher-order phase transition. Our calculated volumetric expansion at zero pressure also compares well with experiment.

The simulated isothermal bulk modulus of $NaMgF_3$ is 81.5 GPa at 300 K and zero pressure, which compares very well with experiment (75.6 GPa [45] and 76.0 GPa [46]). For $KMgF_3$, the calculated isothermal bulk modulus is 86.8 GPa at 300 K. This is somewhat higher than the experimental values of 75.1 GPa [47], 75.6 GPa [48], and 71.2 GPa [26], but the difference does not exceed 20%. It is worth noting in this context that the *ab initio* values of the bulk modulus reported in [26] vary even more, from 72.0 GPa to 91.5 GPa, depending on the exchange-correlation potential used.

Solid Solutions

The $Na_{1-x}K_xMgF_3$ solid solution was simulated at temperatures of 300 K, 500 K, 700 K, and 1000 K for compositions $x = 0$, 0.125, 0.25, 0.375, 0.5, 0.625, 0.75 and 0.875.

We start with the dependence of the lattice parameters on composition which is shown in Figure 6 for several temperatures (300 K, 500 K and 700 K). At room temperature, the transition from the orthorhombic to the cubic structure takes place with increasing potassium concentration at $x \approx 0.5$. This is close to the concentration at which Martin *et al.* [14] report the formation of the cubic phase experimentally, but higher than that in ref. 17 ($x \approx 0.35$) and in ref. 21 ($x \approx 0.22$). At higher temperatures, the system is orthorhombic over progressively smaller ranges of potassium content and in the simulations the orthorhombic structure disappears completely even for $x = 0.125$ above 700 K, in at least qualitative agreement with experiment. The variation of the pseudo-cubic unit cell volume as a function of composition at 300 K is shown in Figure 7. The plot in this figure shows positive deviation from linearity, indicating non-ideal behaviour, consistent with the experiments of Yoshiasa *et al.* [21], and in Figure 8 we examine this further by plotting the excess volume of the solution at all four temperatures as a function of composition. Another key indicator of non-ideality is the enthalpy of mixing and our calculated values as a function of composition and for the same four temperatures is shown in Figure 9. The volumes of mixing are in reasonable agreement with those reported in ref. 21. These, and the positive enthalpies of mixing,

even though these are rather low (≈ 1 kJ/mol even at $x = 0.5$) confirm the non-ideality of the solid solution. Calculations of the free energy (via integration of the chemical potential, following the methods in refs. 30 and 31) indicate full mutual solubility for all compositions at all temperatures considered. This contrasts sharply with the low mutual solubility of the binary fluorides, KF and NaF. The presence of the MgF_6 octahedra in the ternary compound provide a number of strain-relieving mechanisms such as tilting and rotating of the polyhedra which are not available in $Na_{1-x}K_xF$.

The existence of non-ideality naturally raises the question whether clustering of K and Na atoms is taking place in the solid solution. This question was investigated by means of a suitable short-range (SRO) order parameters. We have turned to the Warren-Cowley SRO parameter $\alpha_1(x)$ [49], defined as

$$\alpha_1(x) = 1 - \frac{P_1^{K-Na}}{1-x}, \tag{5}$$

where subscript 1 stands for the number of a coordination sphere (generally, SRO parameter may be defined for an arbitrary coordination sphere, here we are only interested in the first nearest neighbours), and P_1^{K-Na} is the conditional probability of finding a Na atom in the first coordination sphere of K. The SRO parameter $\alpha_1(x)$ is 0 if the probability $P_1^{K-Na} = 1-x$, i.e., if the solution is ideal and the probability is simply that expected for a random distribution consistent with the specified Na content; there is no preference for the K atom to be surrounded by either Na or K. Clustering of K atoms ($P_1^{K-Na} < 1-x$) gives rise to positive values of $\alpha_1(x)$ (repulsive short-range order), while negative values of $\alpha_1(x)$ suggest a tendency toward forming an ordered structure, or attractive SRO. If at low x each K atom were to be surrounded by Na atoms only ($P_1^{K-Na} = 1$), the SRO parameter would take its lowest possible value $\alpha_1(x) = -\left(x/(1-x)\right)$

.

The SRO parameters in $Na_{1-x}K_xMgF_3$ as a function of K content at 300, 500, 700, and 1000 K are shown in Figure 10 and clearly illustrate deviation from ideality. At room temperature, the potassiums show a tendency to cluster together, as seen at the snapshot of the simulation box (Figure 2). This tendency is more pronounced for lower potassium concentrations, and decreases markedly with temperature, virtually disappearing at all

potassium concentrations at 1000 K. This clustering is also evident from the pairwise radial distribution functions (not shown here). The tendency for potassium ions to cluster is consistent with the experimental study of Martin *et al.* [14] who discuss clustering in some detail and relate it to the tilting of the MgF_6 octahedra. A small difference is that while Martin *et al.* suggest clustering of potassium for potassium mole fractions $x < 0.9$, our Figure 10 indicate virtually a random distribution for $x > 0.75$. In our simulations end member local environments are found for all compositions; we have previously emphasised the importance of these local environments in determining solid solutions and non-stoichiometric systems [50].

4. Conclusions

Using a classical ionic model to represent the interactions between the ions, we have performed a detailed exchange Monte Carlo study of the $(K,Na)MgF_3$ solid solution and its end members including high pressures and elevated temperatures. Full account is taken of the local environment of the individual cations, clustering and thermal effects. We suggest the structural transition at high pressures deserves further theoretical study, possibly by *ab initio* methods and perhaps further experimental investigation. The solution is not ideal – our results show that clustering of potassium ions is present, particularly at low temperatures and low K concentrations, which minimizes the total volume and reduces strain.

Acknowledgements

This work was funded in part (MYL) by EPSRC grants GR/M53899 and EP/G050031 and the RCUK Energy Programme (Grant Number EP/I501045). NLA would like to thank Prof. S.P. Gabuda for his outstanding hospitality and scientific insights in many discussions during a visit to Novosibirsk. MYL is happy to remember fruitful discussions and pleasant talks with Prof. S.P. Gabuda spanning a range of almost 30 years.

References

1. L. Liu, *Geophys. Res. Lett.* **2**, 417 (1975).

2. T. Kato and M. Kumazawa, *Nature* **316**, 803 (1985).

3. E. Knittle and R. Jeanloz, *Science* **235**, 668 (1987).

4. J. Zhang and D.J. Weidner, *Science* **284**, 782 (1999).

5. J.P. Brodholt, *Nature* **407**, 620 (2000).

6. C.B. Vanpeteghem, R.J. Angel, N.L. Ross, S.D. Jacobsen, D.P Dobson, K.D. Litasov, and E. Ohtani, *Phys. Earth Planet. Inter.* **155**, 96 (2006).

7. M.J. Gillan, D. Alfè, J. Brodholt, L. Vočadlo, and G.D. Price, *Rep. Prog. Phys.* **69**, 2365 (2006).

8. F. Zhang and A.R. Oganov, *Earth Planet. Sci. Lett.* **249**, 436 (2006).

9. A. Saikia, T.B. Ballaran, and D.J. Frost, *Phys. Earth Planet. Inter.* **173**, 153 (2009).

10. M. Murakami, Y. Ohishi, N. Hirao, and K. Hirose, *Nature* **485**, 90 (2012).

11. E.C.T. Chao, H.T. Evans, Jr., B.J. Skinner, and C. Milton, *Am. Miner.* **46**, 379 (1961).

12. F. Demartin, I. Campostrini, C. Castellano, and M. Russo, *Phys. Chem. Minerals* **41**, 403 (2014).

13. N.L. Allan, M.J. Dayer, D.T. Kulp, and W.C. Mackrodt, *J. Mater. Chem.* **1**, 1035 (1991).

14. C.D. Martin, S. Chaudhuri, C.P. Grey, and J.B. Parise, *Am. Miner.* **90,** 1522 (2005).

15. Y. Zhao, D.J. Weidner, J.B. Parise, and D.E. Cox, *Phys. Earth Planet. Inter.* **76**, 1 (1993).

16. Y. Zhao, D.J. Weidner, J.B. Parise, and D.E. Cox, *Phys. Earth Planet. Inter.* **76**, 17 (1993).

17. Y. Zhao, *J. Solid State Chem.* **141**, 121 (1998).

18. R.W. Smith, W.N. Mei, J.W. Flocken, M.J. Dudik, and J.R. Hardy, *Mat. Res. Bull.* **35**, 341 (2000).

19. A.R. Chakhmouradian, K. Ross, R.H. Mitchell, and I. Swainson, *Phys. Chem. Minerals* **28**, 277 (2001).

20. I.G. Wood, K.S. Knight, G.D. Price, and J.A. Stuart, *J. Appl. Cryst.* **35**, 291 (2002).

21. A. Yoshiasa, D. Sakamoto, H. Okudera, M. Ohkawa, and K. Ota, *Mat. Res. Bull.* **38**, 421 (2003).

22. J. Chen, H. Liu, C.D. Martin, J.B. Parise, and D.J. Weidner, *Am. Miner.* **90**, 1534 (2005).

23. C.D. Martin, W.A. Crichton, H. Liu, V. Prakapenka, J. Chen, and J.B. Parise, *Am. Miner.* **91**, 1703 (2006).

24. R.H. Mitchell, L.M.D. Cranswick, and I. Swainson, *Phys. Chem. Minerals* **33**, 587 (2006).

25. R.H. Mitchell, M. Alexander, L.M.D. Cranswick, and I. Swainson, *Phys. Chem. Minerals* **34**, 705 (2007).

26. G. Vaitheeswaran, V. Kanchana, R.S. Kumar, A.L. Cornelius, M.F. Nicol, A. Svane, A. Delin, and B. Johansson, *Phys. Rev. B* **76**, 014107 (2007).

27. K. Umemoto, R.M. Wentzcovitch, D.J. Weidner, and J.B. Parise, *Geophys. Res. Lett.* **33**, L15304 (2006).

28. J.A. Purton, G.D. Barrera, N.L. Allan and J.D. Blundy, *J. Phys. Chem.* **B102**, 5202 (1998).

29. N.L. Allan, G.D. Barrera, R.M. Fracchia, M.Y. Lavrentiev, M.B. Taylor, I.T. Todorov, and J.A. Purton, *Phys. Rev. B* **63,** 094203 (2001).

30. M.Y. Lavrentiev, N.L. Allan, G.D. Barrera, and J.A. Purton, *J. Phys. Chem. B* **105,** 3594 (2001).

31. I.T. Todorov, N.L. Allan, M.Y. Lavrentiev, C.L. Freeman, C.E. Mohn and J.A. Purton, *J. Phys.: Condens. Matter* **16**, S2751 (2004)

32. C.E. Mohn, M.Y. Lavrentiev, N.L. Allan, E. Bakken and S. Stølen, *Phys. Chem. Chem. Phys.* **7**, 1127 (2005).

33. D. Frenkel and B. Smit, *Understanding Molecular Simulation*, 2nd ed., Academic Press, San Diego (2002).

34. N. Metropolis, A.W. Rosenbluth, M.N. Rosenbluth, A.H. Teller, and E. Teller, *J. Chem. Phys.* **21**, 1087 (1953).

35. M.Y. Lavrentiev, J.A. Purton, and N.L. Allan, *Am. Miner.* **88**, 1522 (2003).

36. M.Y. Lavrentiev, W. van Westrenen, N.L. Allan, C.L. Freeman, and J.A. Purton, *Chem. Geol.* **225**, 336 (2006).

37. *Computer Simulation of Solids*, Ed. C.R.A. Catlow and W.C. Mackrodt, Springer-Verlag (1982).

38. N.L. Allan, M. Braithwaite, D.L. Cooper, W.C. Mackrodt and B. Petch, *Mol. Simul.* **9**, 161 (1992)

39. N.L. Allan, M. Braithwaite, D.L. Cooper, W.C. Mackrodt and B. Petch, *J. Chem. Soc., Faraday Trans.* **89**, 4369 (1993)

40. F. Claeyssens, J.M. Oliva, D. Sánchez-Portal and N.L. Allan, *Chem. Commun.*,

2440-2441 (2003)

41. E. Rönnebro, D. Noréus, K. Kadir, A. Reiser, and B. Bogdanovic, *J. Alloys Comp.* **299**, 101 (2000).

42. A.G. Bergman and E.P. Dergunov, *Compt. Rend. Acad. Sci. U.S.S.R.* **31**, 755 (1941).

43. R.C. DeVries and R. Roy, *J. Am. Chem. Soc.* **75**, 2479 (1953).

44. Y. Zhao, D.J. Weidner, J. Ko, K. Leinenweber, X. Liu, B. Li, Y. Meng, R.E.G. Pacalo, M.T. Vaughan, Y. Wang, and A. Yeganeh-Haeri, *J. Geophys. Res.* **99**, 2871 (1994).

45. Y. Zhao and D.J. Weidner, *Phys. Chem. Minerals* **20**, 419 (1993).

46. H.-Z. Liu, J. Chen, J. Hu, C.D. Martin, D.J. Weidner, D. Häusermann, and H.-K. Mao, *Geophys. Res. Lett.* **32**, L04304 (2005).

47. L.M. Reshchikova, *Sov. Phys. – Solid State* **10**, 2019 (1969).

48. L.E.A. Jones, *Phys. Chem. Minerals* **4**, 23 (1979).

49. J.M. Cowley, *Phys. Rev.* **77**, 669 (1950).

50. N.L. Allan, S. Stølen and C.E. Mohn, *J. Mat. Chem.* **18,** 4124 (2008)

Table 1

Potential	A (/eV)	ρ (/Å^{-1})	C (/(eV Å^6))
Mg - F	3962.69	0.2267	0.1
Na - F	2980.50	0.23677	1.41725
K - F	3441.43	0.265364	8.162418
F - F	654.113	0.2885	7.14561

Potentials used in this work. Electron-gas potentials were fitted to Buckingham functional forms ($V(r) = \exp(-r/\rho) - Cr^{-6}$). A cut-off of 10 Å was used.

Table 2

$KMgF_3$

Parameters	Experimental	Calculated
a / Å	5.6423[(a)] 5.6339[(b)]	5.630884
b / Å	5.6423[(a)] 5.6339[(b)]	5.630884
c / Å	7.9794[(a)] 7.9676[(b)]	7.963268
V / Å^3	254.03[(a)] 252.90[(b)]	252.49011
K *x*	1.0	1.0
K *y*	0.0	0.0
K *z*	0.25	0.25
Mg *x*	0	0
Mg *y*	0.5	0.5
Mg *z*	0	0
F1 *x*	0.0	0.0
F1 *y*	0.5	0.5
F1 *z*	0.25	0.25
F2 *x*	0.75	0.75
F2 *y*	0.25	0.25
F2 *z*	0.0	0.0

$NaMgF_3$

Parameters	Experimental	Calculated
a / Å	5.3607[(a)] 5.3606[(b)] 5.3579[(c)] 5.3617[(d)]	5.354195
b / Å	5.4873[(a)] 5.4873[(b)] 5.4842[(c)] 5.4897[(d)]	5.466473
c / Å	7.6662[(a)] 7.6668[(b)] 7.6618[(c)] 7.6682[(d)]	7.647191
V / Å^3	225.51[(a)] 225.52[(b)] 225.13[(c)] 225.71[(d)]	223.82227
Na *x*	0.9895[(a)] 0.9893[(c)] 0.9902[(d)]	0.990349
Na *y*	0.0441[(a)] 0.0443[(c)] 0.0446[(d)]	0.038510
Na *z*	0.25	0.25
Mg *x*	0	0
Mg *y*	0.5	0.5
Mg *z*	0	0
F1 *x*	0.0897[(a)] 0.0865[(c)] 0.0877[(d)]	0.088344
F1 *y*	0.4722[(a)] 0.4716[(c)] 0.4730[(d)]	0.466976
F1 *z*	0.25	0.25
F2 *x*	0.7028[(a)] 0.7031[(c)] 0.7025[(d)]	0.705824
F2 *y*	0.2964[(a)] 0.2953[(c)] 0.2949[(d)]	0.292255
F2 *z*	0.0476[(a)] 0.0468[(c)] 0.0459[(d)]	0.046750

Table 2. Experimental and calculated structural parameters for the end members $KMgF_3$ and $NaMgF_3$. Experimental data are from Chakhmouradian *et al.* [19] (a), Martin *et al.* [14] (b), Zhao *et al.* [15] (c), Rönnebro *et al.* [41] (d).

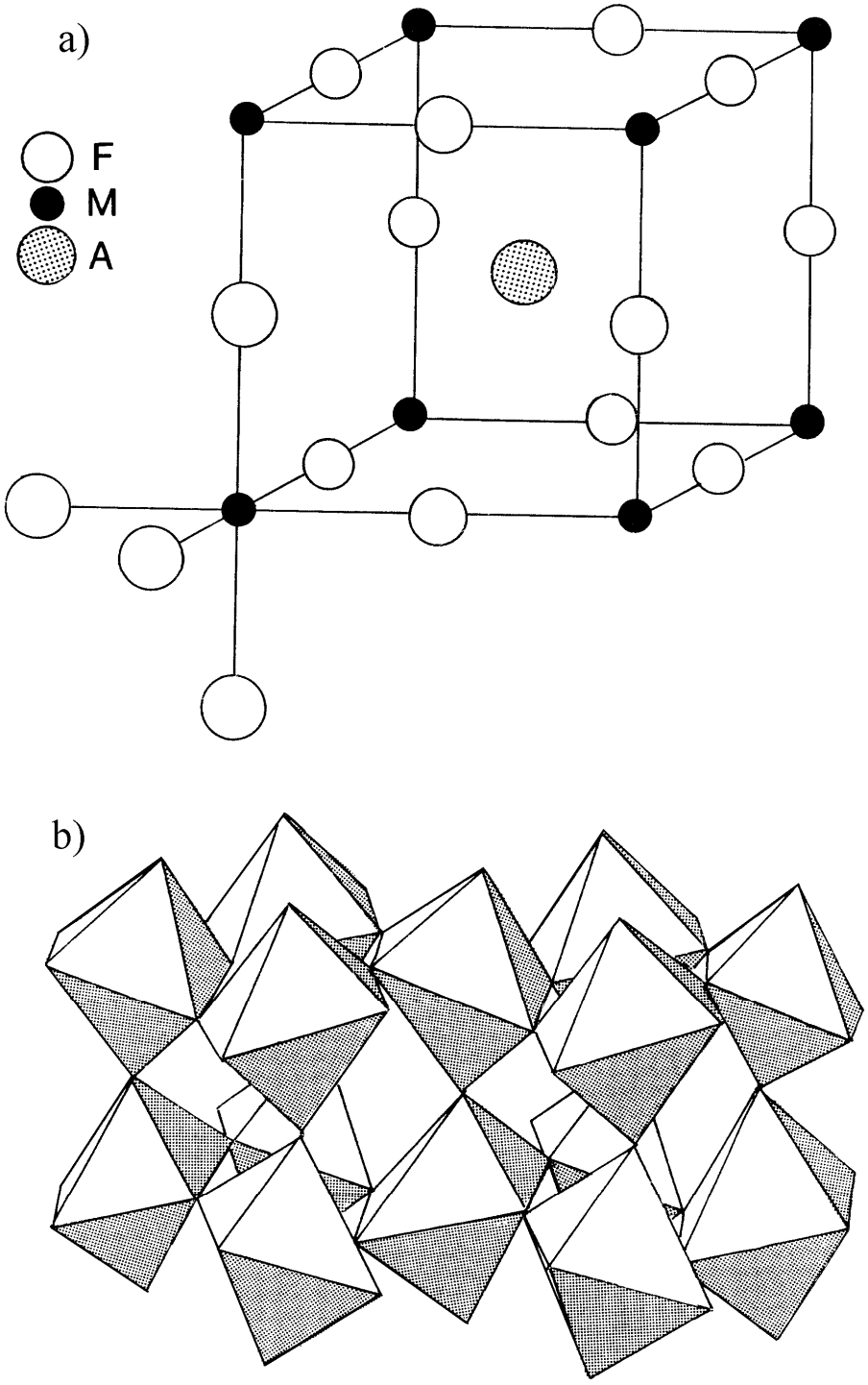

Figure 1 a) Cubic perovskite structure AMF_3 b) Representative tilting of MF_6 octahedra in an orthorhombic perovskite.

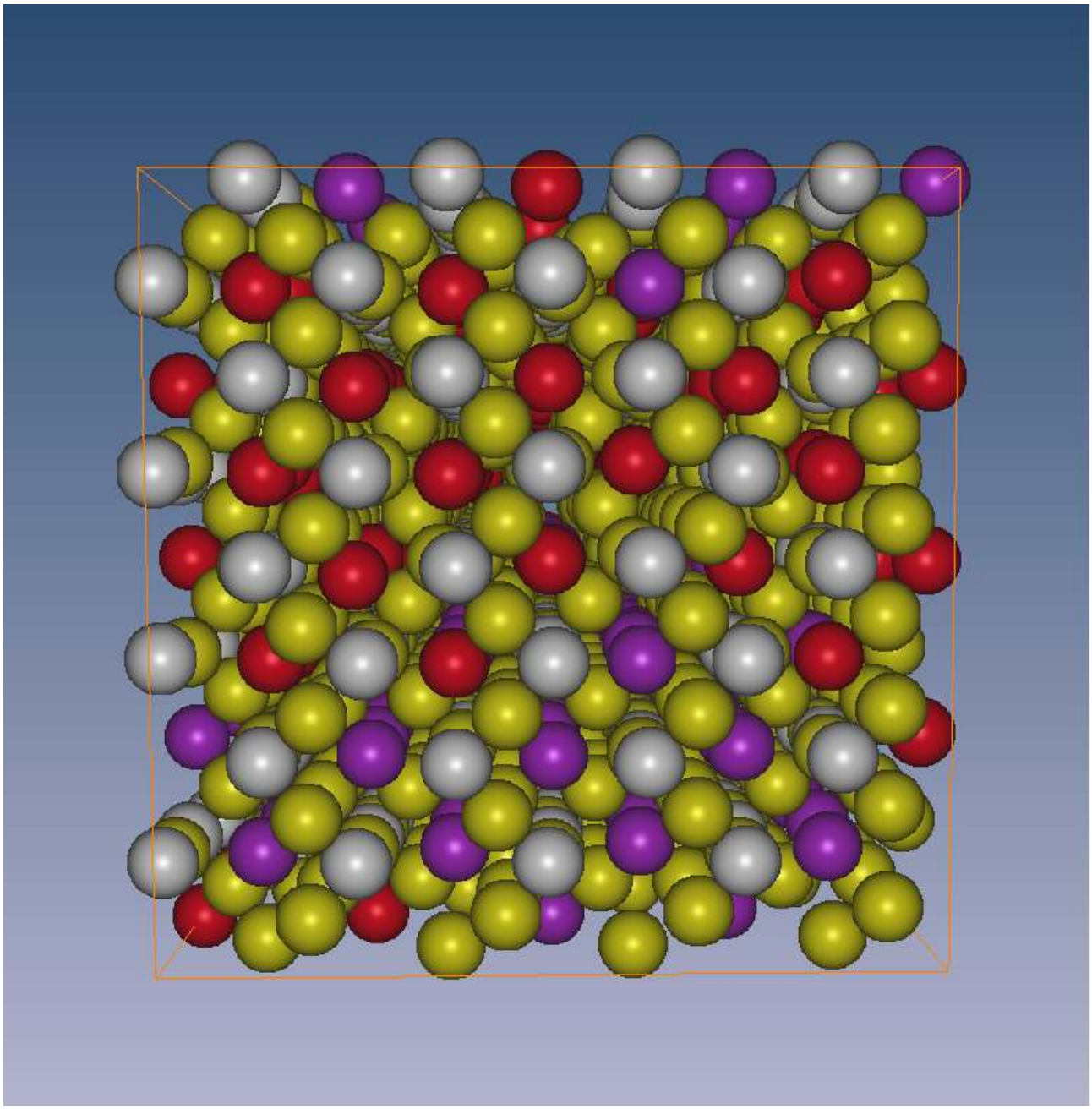

Figure 2
Snapshot of the Monte Carlo simulation box (1280 atoms) of the $Na_{1-x}K_xMgF_3$ solid solution at K content $x = 0.5$ and temperature T = 300 K. Violet atoms are K^+, red Na^+, silver Mg^{2+} and olive green F^-.

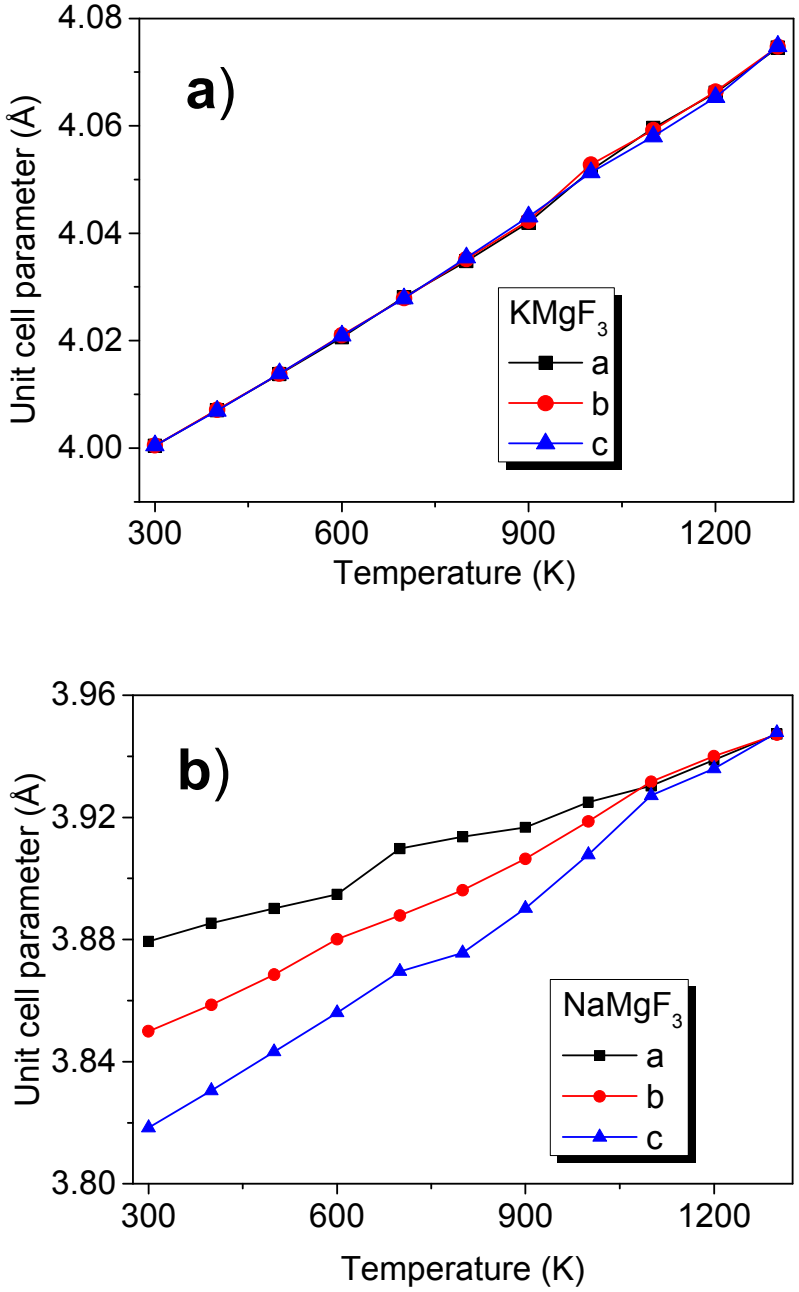

Figure 3
Temperature dependence of the pseudo-cubic unit cell parameters (Å) ($a = a'/2^{1/2}$, $b = b'/2^{1/2}$, $c = c'/2$) for the end-members $KMgF_3$ (a) and $NaMgF_3$ (b). For $KMgF_3$, the three pseudo-cubic parameters almost coincide, indicating a cubic unit cell.

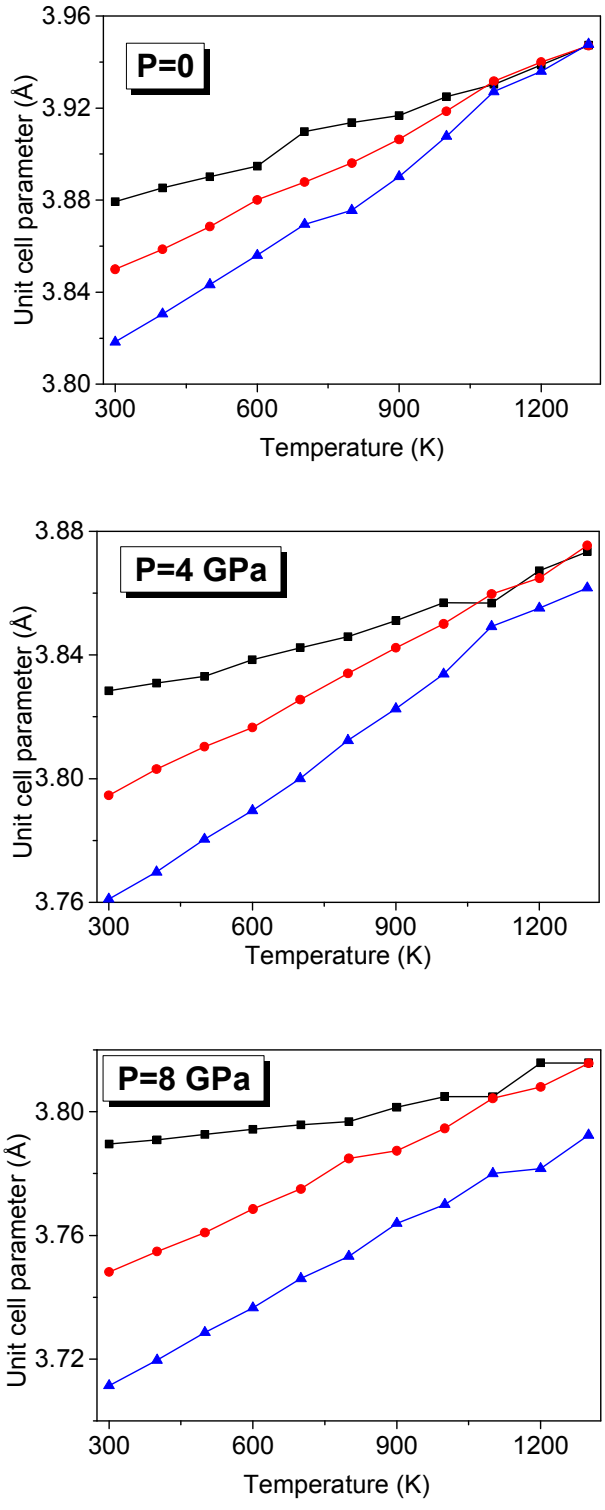

Figure 4
Temperature dependence of the pseudo-cubic unit cell parameters (Å) for $NaMgF_3$ at pressures of 0, 4, and 8 GPa. Unlike the zero pressure results, at high pressures and temperatures above 1000 K only two of the three parameters coincide, indicating a tetragonal phase.

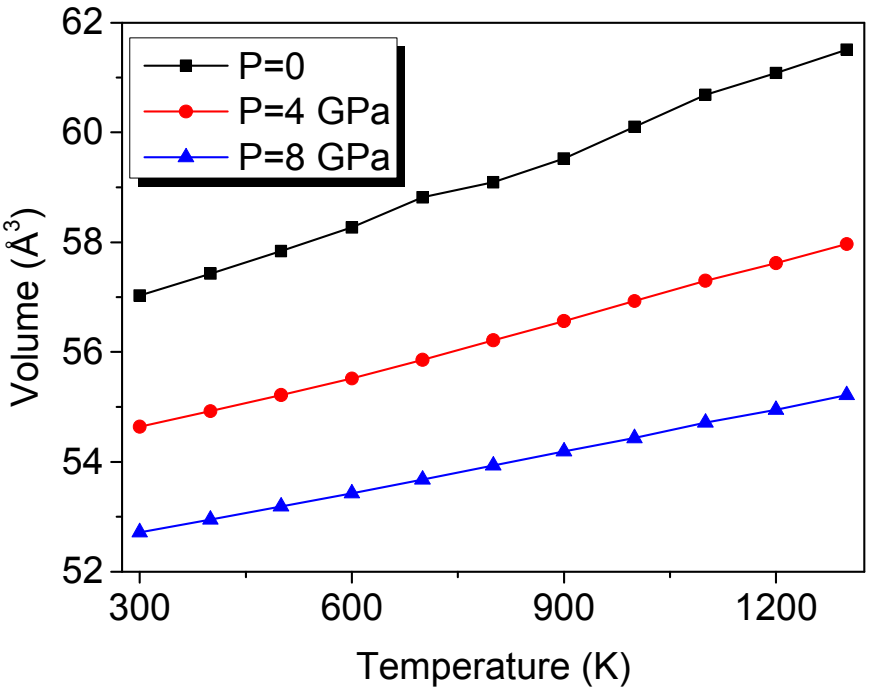

Figure 5
Temperature dependence of the pseudo-cubic cell volume (Å^3) for $NaMgF_3$ at 0, 4 and 8 GPa.

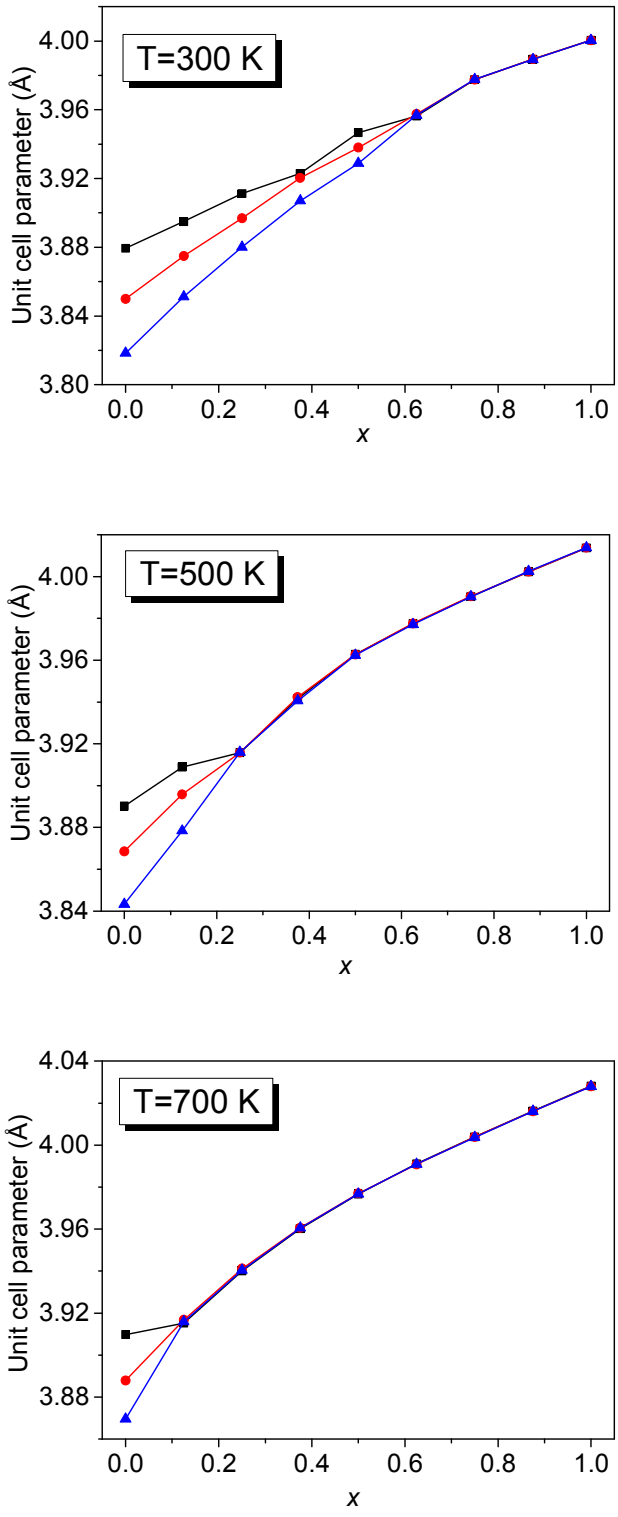

Figure 6
Variation of the pseudo-cubic cell parameters (Å) as a function of K content, *x*, for the solid solution $Na_{1-x}K_xMgF_3$ at 300 K, 500 K, and 700 K. The range of concentrations at which the system is orthorhombic decreases as the temperature increases. Estimated uncertainties in the calculated cell parameters are less than 0.001 Å.

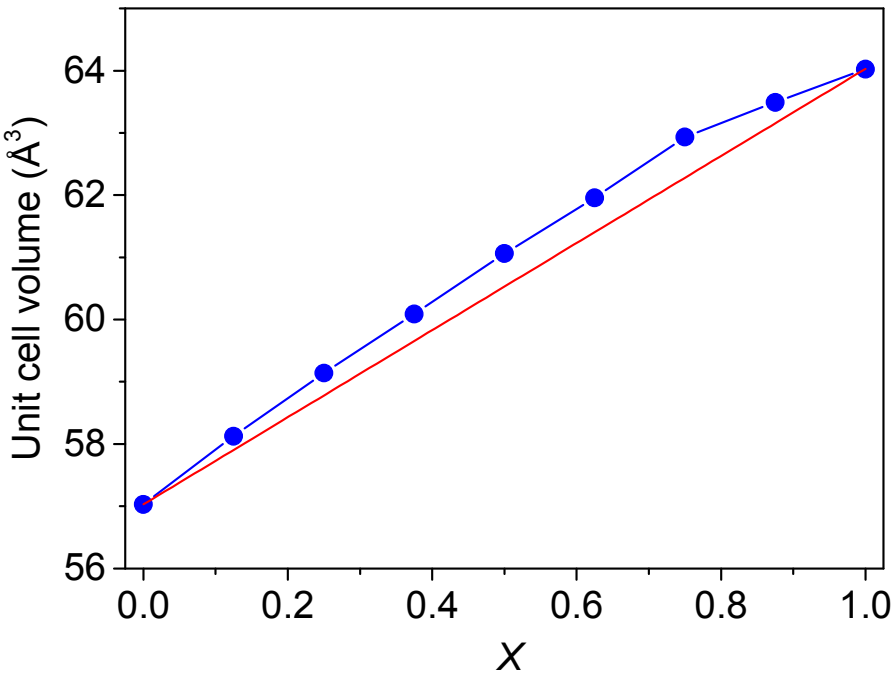

Figure 7
Variation of the pseudo-cubic volume (Å^3) as a function of K content, *x*, for the solid solution $Na_{1-x}K_xMgF_3$ at 300 K (blue circles). The red straight line between the end members is that expected for an ideal solution.

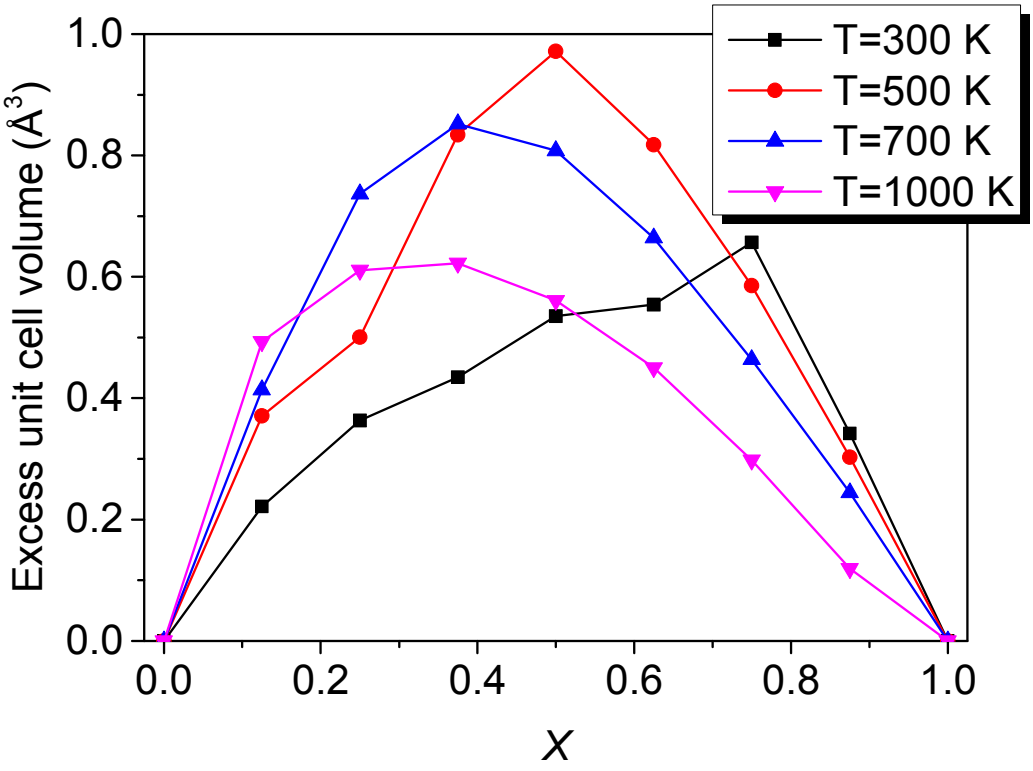

Figure 8
Excess volume of the $Na_{1-x}K_xMgF_3$ solid solution ($Å^3$) as a function of K mole fraction, *x*, at 300, 500, 700 and 1000 K.

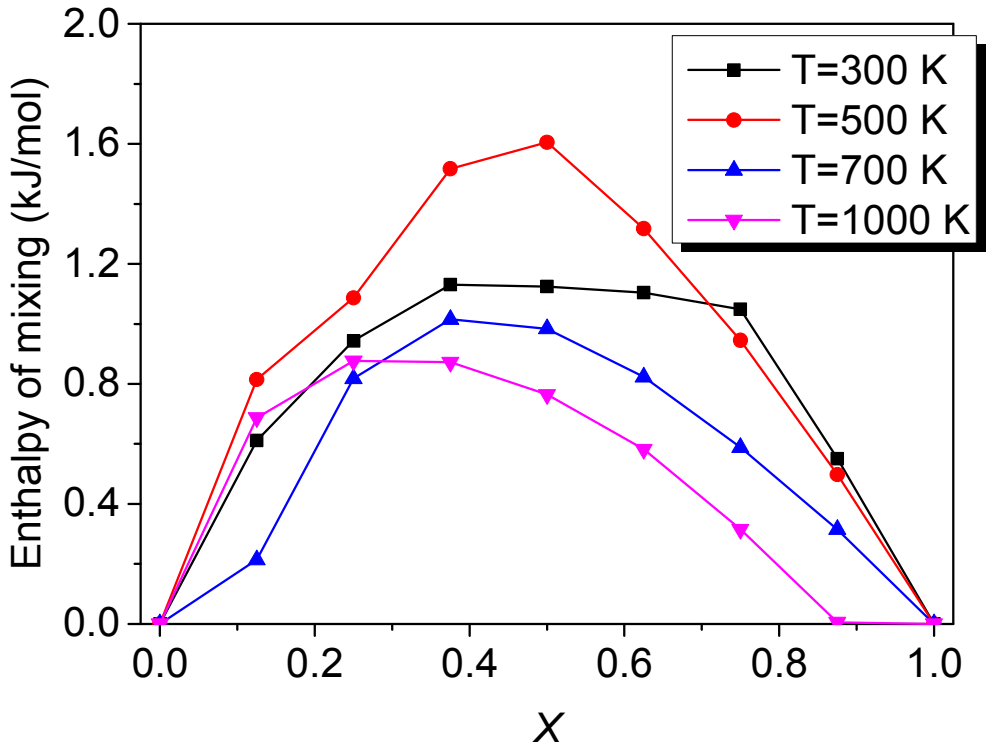

Figure 9
Enthalpy of mixing of the $Na_{1-x}K_xMgF_3$ solid solution (kJ/mol) as a function of K mole fraction, x, at 300, 500, 700 and 1000 K. Estimated uncertainties are less than 0.02 kJ/mol.

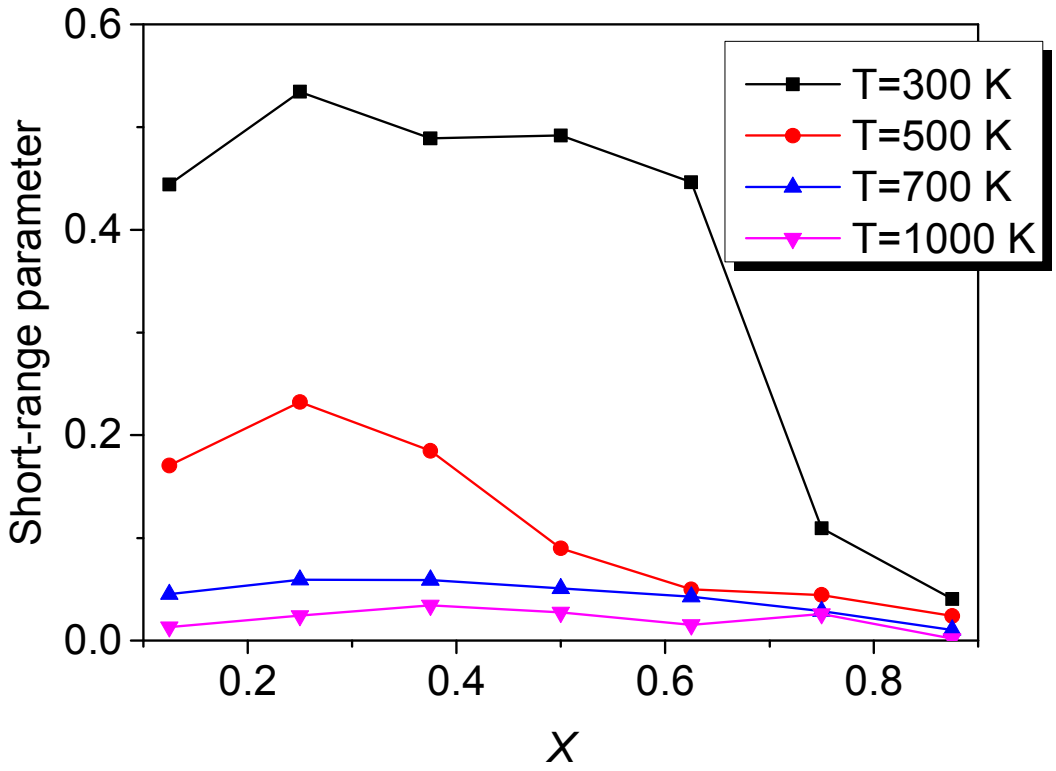

Figure 10

K-Na short range order parameters as a function of K content, *x,* at zero pressure at 300, 500, 700, and 1000 K.